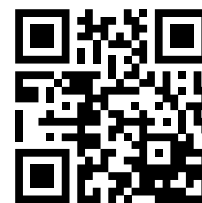


# [8] Simulation model of a multichannel Offner hyperspectrometer

A.D. Golovin, A.V. Demin

ITMO University (Saint Petersburg National Research University  
of Information Technologies, Mechanics and Optics), Saint Petersburg, Russia



## Abstract

We study an advanced airborne hyperspectral system based on the Offner scheme for Earth remote sensing that has the advantages of compact size and high spatial and spectral resolution. An algorithm that enables choosing the most effective design parameters is developed. A schematic design and a simulation model of the multichannel hyperspectrometer are discussed.

**Keywords:** *OFFNER'S ANASTIGMAT, HYPERSPECTROMETER, ROWLAND CIRCLE, CONVEX GRATING, REMOTE SENSING OF THE EARTH.*

**Citation:** *GOLOVIN A.D. SIMULATION MODEL OF A MULTICHANNEL OFFNER HYPERSPECTROMETER /*

*GOLOVIN A.D., DEMIN A.V. //*

*COMPUTER OPTICS. – 2015. – VOL. 39(4). P. 521-528*

## Introduction

There is currently a growing demand on the part of various authorities for space-based observations, first of all, for images of objects of interest and areas of the earth's surface. A rapid sales growth may be observed in the international market of remote sensing of the Earth from space, and the leading space nations conduct remote sensing of different areas of the earth's surface for commercial purposes [1].

It is obvious that when developing high-information space-borne systems, it is necessary to focus on the most advanced optical technologies and new methods thus to solve recognition problems. The fact of proceeding to hyperspectral images of investigated scenes in space-borne electrooptical systems and to spectral-topological image recognition enables to solve, using small spacecrafts (SC), many of those problems which were previously solved by heavy spacecrafts equipped with large-sized panchromatic optical systems [2].

The main idea for hyperspectral systems is a spectral signature concept, i.e. for any proper material, based on an appropriate physical structure and chemistry, the electromagnetic radiation (EMR) quantity to be reflected, radiated, transferred or absorbed thereby, shall be changed in accordance with a radiation wavelength.

Based on gathered data, a 'data cube' (or an 'image cubic model') which reflects objects and information inaccessible for conventional multispectral scanners shall be created. To complete a hypercube, the investigated scene is usually scanned along the direction of a moving platform, and the second dimension of the detector shall simultaneously collect all spectral information [3]. The main advantage of this mode is synchronism in a linearly dispersed spectrum with no post-processing required, except for correction of atmospheric distortions. Among all feasible architectures of hyperspectrometers, the Offner scheme is the most advanced due to its simplicity, small dimensions and high optical indices. This paper describes the evolution of the development of this scheme and considers in detail, due to what modifications it is possible to achieve a good image quality within rather a wide spectral range, thus maintaining compact sizes of the hyperspectrometer [4].

### 1. The Offner's mirror anastigmat

The Offner mirror system is a completely reflecting telecentric system required for obtaining off-axis objects. It was developed by Abe Offner as a mask plane relay with respect to the target alignment for optical printing of integrated circuits.

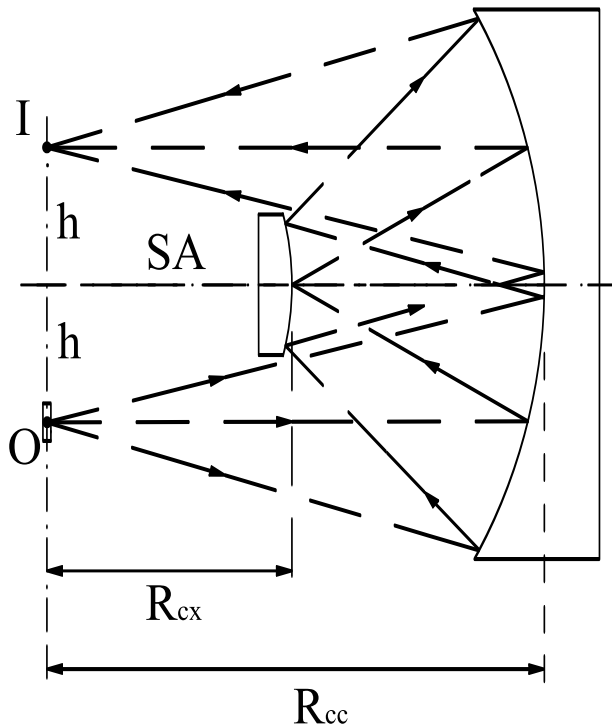


Fig.1. The Offner mirror system

The mirrors are placed with a center of curvature in the point P, and they contain off-axis codomains with their centers in the points O and I (Fig.1). The points O and I are located on opposing sides of the optical axis SA at the distance H. A concave mirror forms the image I of the object O. A convex mirror forms a false image I in the point O which is reflected by the concave mirror. If the radius of curvature of the concave mirror is twice as large as the radius of curvature of the convex mirror, the algebraic sum of optical powers of reflecting surfaces become zero, because the concave mirror may produce two reflections.

After that, the system corrects all Seidel aberrations; only the fifth-order field curvature stays essential, which may be corrected by increasing the radius of the convex mirror in accordance with the Petzval condition. The system given in Fig.1 becomes afocal at the height of h, whereby the focusing or longitudinal interface position errors do not affect the system power [5, 6].

This combination is free from spherical aberration, coma and distortion, and when the algebraic sum of degrees of mirror reflection surfaces becomes zero, the resultant image will be free from the third-order astigmatism and field curvature. This system is independent from the spectral region which is used in the imagery,

and the contrast range therein is uniformly high and substantially constant within the whole field region.

To perform as a dispersion spectrometer, the second convex mirror in the Offner projection system was replaced by a convex diffraction grating, the grooves of which were parallel to an entrance slit. Usually, in similar schemes, the increase of spectrometer dimensions for a proper size of the slit can reduce a field slope angle, so it may result in the reduction of field aberrations, such as astigmatism. M.P.Chrisp [7] proposed to replace the first concave mirror by two individual ones  $M_1$  and  $M_2$ , thus having arranged all spherical elements on certain Rowland circles, which intersect in a single center of curvature and in the field of the false image of the diffraction grating. Centers of curvature of the mirrors and the grating, as well as a focal plane and a slit center are to be placed in the same plane. Radii of curvature for the mirrors  $M_1$  and  $M_2$  have been selected independently of one another and are equal to  $R_1 = 2R_{gr} \cos(\alpha/2)$  and  $R_2 = 2R_{gr} \cos(\beta/2)$ , respectively, where  $R_{gr}$  is the radius of the diffraction grating, and  $\alpha$  and  $\beta$  are the angles between the incidence and reflected beams at the poles of the convex mirrors. Taking into account these modifications, the aberrations of defocusing, astigmatism and coma are to be corrected with no increase of the spectrometer size required for the given slit size. Thus, the spectrometer compact size is maintained, that was hardly achieved in standard spectrometers providing herewith a good quality of spatial and spectral images on the detector's focal plane.

## 2. The multichannel hyperspectrometer

It is a good practice to use a blazed grating (with a small blazing angle) in contemporary spectrometer systems, since it possesses the property of high energy concentration in a certain spectral order (up to 90%). This grating can't be obtained by threading with a ruling machine, because a tool angle can't be continuously changed within each groove [8]. The electron-beam lithography approach offers comparatively a new method to fabricate gratings on convex planes, which make it possible to control a groove form in order to provide the given curve of diffraction efficiency and to develop multi-panel gratings of arbitrary shapes, intervals and number of grooves. Several blaze regions, being completely flexible in their

shaping, can easily be used in designing [9–11]. Manufacturing of these gratings makes it possible to create the multichannel hyperspectrometer based on the above scheme. It includes one or more entrance slits one per each channel. The light transmitted through the slits is reflected by the first concave mirror to the convex grating which disperses the light into two respective spectra. Being reflected from the second concave mirror, the spectra shall come on an image sensor. The entrance slits are displaced on Y-axis with respect to each other. Resulting from this displacement, the obtained spectra are separately reflected on the image sensor, so that at least the respective parts of two spectra do not overlap and may be separately imaged by means of the image sensor.

The entrance slits are also displaced horizontally on X-axis with respect to each other. As a result of this displacement, the light falls from two input channels on the convex diffraction grating at the respective different incidence angles  $\alpha_1$  and  $\alpha_2$  (Fig.2). The contrasting incidence angles  $\alpha_1$  and  $\alpha_2$  result to the fact that various light wavelengths will be diffracted at various diffraction angles  $\alpha'$  from the diffraction grating in accordance with the following diffraction grating formula [12]:

$$\sin \alpha + \sin \alpha' = k\lambda m, \quad (1)$$

where  $\alpha$  is the incidence angle,  $\alpha'$  is the diffraction angle of the maximum order  $k$ ,  $\lambda$  is the wavelength of a diffracted beam and  $m$  is the number of grooves per unit length ( $m = 1/b$ , where  $b$  is the distance between neighboring grooves). It follows from this formula that the light with a larger wavelength is diffracted at relatively small angles such as  $\alpha'_1$ , whereas the short-wave light is diffracted at relatively large angles, such as  $\alpha'_2$ . The light reflection from each grating groove shall produce an individual light beam. Occurrence of the constructive interference shall increase the given wavelength intensity if the distance between two parallel beams differs in length by a wavelength integer multiple, whereas the destructive interference shall usually cancel other light wavelengths. Thus, the beams reflected at other angles shall basically contain the light of other respective wavelengths, and rays of the parallel light beams shall mainly contain the same light wavelength. The light obtained from the first slit, which was diffracted at each angle  $\alpha'$ , has a larger wavelength compared with the light transmitted into the second slit and diffracted at the same angle  $\alpha'$ .

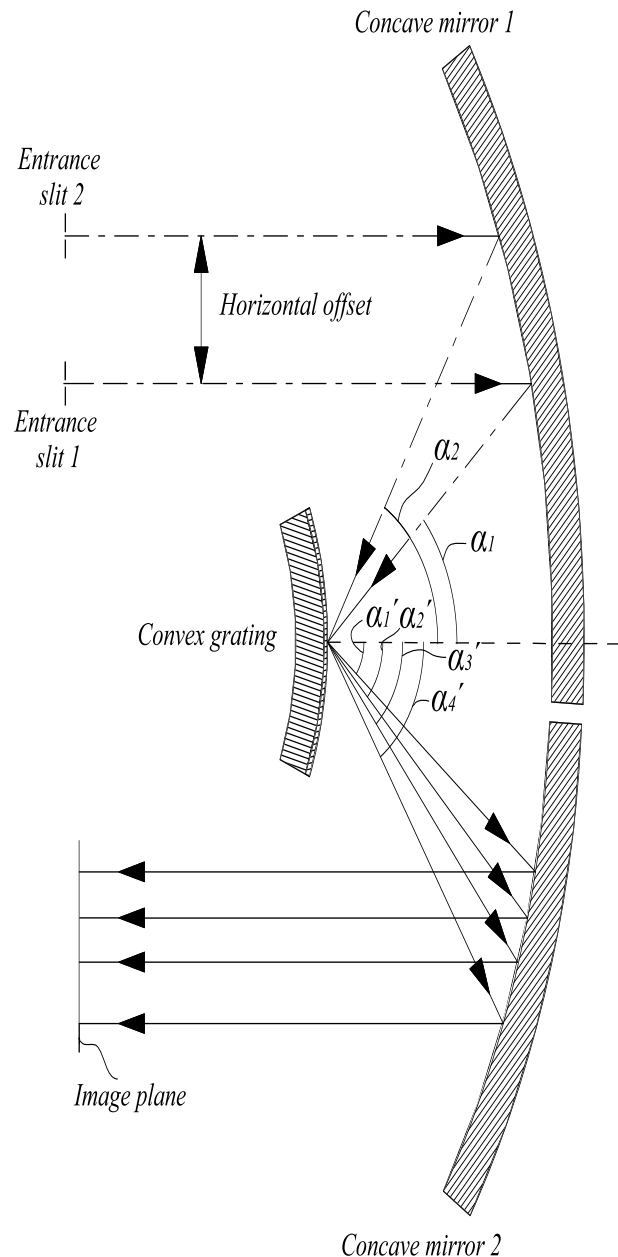


Fig.2. Spectra imaging. Cross-sectional view of a hyperspectrometer's part.

As is shown in Fig. 2, each dispersive spectrum shall account for an infinite number of diffraction angles of two different wavelengths of the diffracted light (as example of  $\alpha'_1$ ,  $\alpha'_2$ ,  $\alpha'_3$  and  $\alpha'_4$ ). Resulted from the light diffracted from the first slit, the first spectrum is formed in the plane of the image sensor, and the second spectrum is formed from diffraction of the light transferred from the second slit.

### 3. Calculation theory

The geometric calculation of the system may be per-

formed by means of the wave front decomposition in meridian and sagittal sections with a coordinates system in the center of curvature of the mirrors.

The meridian image of a point object obtained by a reflection grating shall satisfy the following equation [13]:

$$\frac{\cos^2 \alpha}{r} + \frac{\cos^2 \alpha'}{r'_m} = \frac{\cos \alpha + \cos \alpha'}{R} \quad (2)$$

and the sagittal image shall satisfy the following equation:

$$\frac{1}{r} + \frac{1}{r'_s} = \frac{\cos \alpha + \cos \alpha'}{R} \quad (3)$$

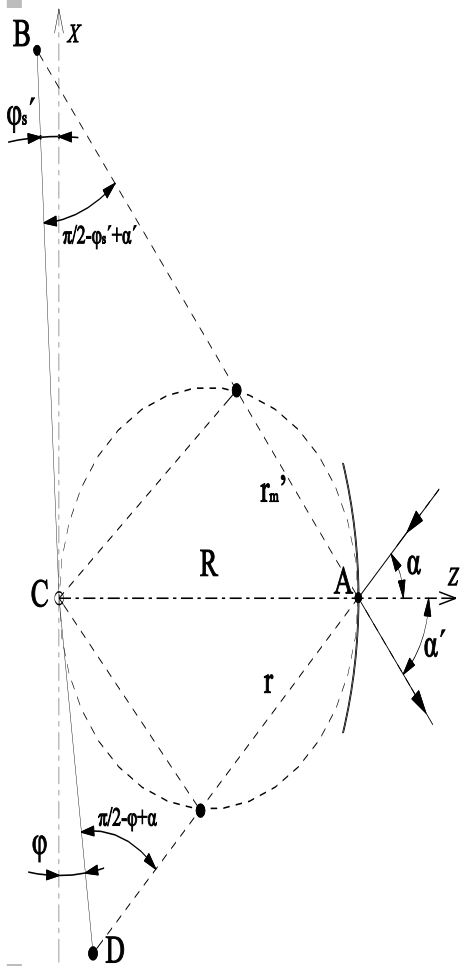


Fig.3. Positioning meridian and sagittal images through the grating for an imaginary object point

In these equations R is the radius of curvature of the diffraction grating;  $r'_m$  and  $r'_s$  are the distances from the main beam incidence point to the grating prior to the object, both in the meridian ( $r'_m$ ), and sagittal ( $r'_s$ ) image points (see Fig. 3). This particular configuration shall meet the Rowland condition [14]:

$$r = R \cos \alpha \Rightarrow r'_m = R \cos \alpha' \quad (4)$$

In this case the object and its meridian image lie in the circle of R/2 radius, which contain the center of curva-

ture of the grating and the entrance slit (the Rowland circle), as is shown in Fig. 3.

However, as can be seen from the equation (3), the sagittal image does not lie in this circle, that makes astigmatism the most important aberration. From ACB and ACD triangles, using the sine theorem, we obtain the following:

$$\frac{1}{r} = \frac{\cos(\varphi - \alpha)}{R \cos \varphi}$$

$$\frac{1}{r'} = \frac{\cos(\varphi'_s - \alpha')}{R \cos \varphi'_s} \quad (5)$$

Replacement of the formulas (5) in the equation (3) results in the following invariant (K) for the sagittal image:

$$K = \sin \alpha \tan \varphi = -\sin \alpha' \tan \varphi'_s \quad (6)$$

A sufficient criterion for the Rowland condition proposing the image without coma is the fact that the object point and, at the same time, final and intermediate images were in the Rowland circle of each element, subject to the condition that the object point is arranged in the first Rowland circle. Let us consider this condition in a geometric shape. Fig. 4 shows the Rowland circle consisting of three elements, the center of total curvature (C), and the object point (O) and both (IM) meridian images (intermediate and final) are situated in these circles. The object is placed in the first Rowland circle, if the angle between CO and the main beam is equal to  $\pi/2$ . This follows from the trigonometric property which reads that the triangle is right if its hypotenuse is the diameter for its escribed circle.

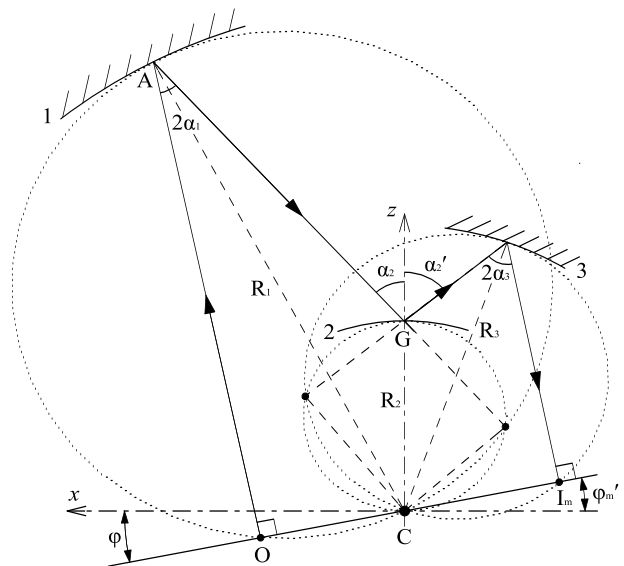


Fig.4. The Rowland circles indicating the location of the meridian image

Having taken the AOCG tetragon, we obtain the following:

$$\frac{\pi}{2} - 2\alpha_1 + (\pi - \alpha_2) + \frac{\pi}{2} + \varphi = 2\pi \Rightarrow \varphi = \alpha_2 + 2\alpha_1. \quad (7)$$

Note that  $\alpha_1 < 0$ . Besides, the CO distance can be written as follows:

$$CO = R_1 \sin \alpha_1 = -R_2 \sin \alpha_2, \quad (8)$$

where the last equation holds true, since the first and the second Rowland circles intersect in the meridian image of the main mirror. In the same way we obtain the following mathematical conditions for the final location of the meridian image:

$$\frac{\pi}{2} - 2\alpha_3 + (\pi - \alpha'_2) + \frac{\pi}{2} - \varphi'_m = 2\pi \Rightarrow \varphi'_m = \alpha'_2 - 2\alpha_3 \quad (9)$$

$$CI_m = R_2 \sin \alpha'_2 = R_3 \sin \alpha_3 \quad (10)$$

We can correlate amplitudes of both object points and the final sagittal image with the angles of incidence and refraction on the grating using the following equation (6):

$$\sin \alpha_2 \tan \varphi = -\sin \alpha'_2 \tan \varphi'_s \quad (11)$$

On the other hand, radial locations of the sagittal image may be correlated with meridian points as follows:

$$CI_s = \frac{CI_m}{\cos(\varphi'_m - \varphi'_s)} \quad (12)$$

Having tracked location of final meridian and sagittal images, it would not be difficult to identify astigmatism as the distance therebetween:

$$\Delta = CI_s \sin(\varphi'_m - \varphi'_s) \quad (13)$$

Therefore, the condition for achieving zero astigmatism for the given wavelength (which may be taken as a mean from the spectral range of the spectrometer) is as follows:

$$\overline{\varphi}' = \overline{\varphi}'_s = \overline{\varphi}'_m = \overline{\alpha}'_2 - 2\overline{\alpha}'_3 \quad (14)$$

If that is so, then it is clear from the above equation (12) that:

$$\overline{CI} = \overline{CI}_m = \overline{CI}_s \quad (15)$$

Due to dispersion of the diffraction grating, the meridian and sagittal images are considered, in actual truth, to be the curves in place of the points. The above equation (14) ensures only zero astigmatism along the wavelength  $\overline{\lambda}$ , where the curves intersect. Having made the meridian and sagittal curves tangential to each other on the wavelength  $\overline{\lambda}$ , we can eliminate astigmatism for other wavelengths. Mathematically, the tangency condition means that astigmatism (the distance between the curves along the main beams) gives at least the second wavelength order. Thus, we can assume the following:

$$\left. \frac{d\Delta}{d\lambda} \right|_{\overline{\lambda}} = 0 \Rightarrow \left. \frac{d(\varphi'_m - \varphi'_s)}{d\alpha'_2} \right|_{\overline{\alpha}'_2} = 0 \quad (16)$$

where we use the equations (13) and (14). A derivative of the meridian angle is determined by the equations (9) and (10):

$$\frac{d\varphi'_m}{d\alpha'_2} = 1 - 2 \frac{\tan \alpha_3}{\tan \alpha'_2} \quad (17)$$

whereas the equation (11) enables to obtain the following:

$$\frac{d\varphi'_s}{d\alpha'_2} = -\frac{\sin \varphi'_s \cos \alpha_3}{\tan \alpha'_2} \quad (18)$$

Connecting the last two equations and using the above formula (14), thus to exclude  $\alpha'_2$ , let's write the above equation (16) as follows:

$$\tan(\overline{\varphi}' + 2\overline{\alpha}_3) - 2 \tan \overline{\alpha}_3 + \frac{\sin 2\overline{\varphi}'}{2} = 0 \quad (19)$$

The first and the second members may be written as the functions of  $\tan \overline{\varphi}'$ . After some algebraic transformations to be made, the cubic equation through  $\tan \overline{\varphi}'$  will be as follows:

$$\frac{\sin^3 \overline{\alpha}_3}{\cos \overline{\alpha}_3} + \tan \overline{\varphi}' - \tan \overline{\alpha}_3 \cos(2\overline{\alpha}_3) \tan^2 \overline{\varphi}' + \frac{1 + 2 \sin^2 \overline{\alpha}_3}{2} \tan^3 \overline{\varphi}' = 0$$

This (20) equation has only one real solution for  $\tan \overline{\varphi}'$ . The n-order solution is as follows (21):

$$\tan \overline{\varphi}'_n = -\frac{\sin^3 \overline{\alpha}_3}{\cos \overline{\alpha}_3} + \tan \overline{\alpha}_3 \cos(2\overline{\alpha}_3) \tan^2 \overline{\varphi}'_{n-1} - \frac{1 + 2 \sin^2 \overline{\alpha}_3}{2} \tan^3 \overline{\varphi}'_{n-1},$$

at  $\overline{\varphi}'_0 = 0$ . For typical values  $\overline{\alpha}_3$  ( $\overline{\alpha}_3 < 30^\circ$ ),  $\overline{\varphi}'$  is less than 0.1 rad; hence, it may be quickly solved using the iteration method [15].

To accomplish theoretical calculations for the hyperspectrometer Offner the final ratio is to be derived connecting the spectrometer size with the period of diffraction grating. We can find a maximum permissible grating width using the following formula:

$$L_{\max} = 2R_2 \cdot 4 \sqrt{\frac{2\Delta\lambda}{r \cdot \sin^2 \alpha_2 + r'_m \cdot \sin^2 \alpha'_2}} \quad (22)$$

The grating radius  $R_2$  shall be selected in accordance with its dimensions and a minimum half width of the hardware function to be achieved. A spectral instrument is characterized with a value called the 'linear dispersion':

$$(dl/d\lambda)_{\min} = kmR_{gr} \quad (23)$$

where  $d\lambda$  is the length of the selected spectral range and  $dl$  is the width of a radiation receiver. The dispersion shall reach its minimum value nearby a normal to the grating; in this region it depends almost not at all on the light wavelength; this spectrum is called normal. If we know the linear dispersion, we may calculate the period  $m$  required for diffraction grating as follows:

$$m = \frac{dl \cdot n}{d\lambda \cdot R_2} \quad (24)$$

#### 4. Mathematical simulation of the hyperspectrometer

We have chosen a focal number  $f/4$  because this is a standard value for this type of imaging spectrometers [16]. In the case of our hyperspectrometer, it was accepted that the diffraction grating was manufactured based on the e-beam lithography technology, and it has a triangle profile with a small blazing angle [17–19]. In designing a grating profile we used PCGrate-S(X) software, the algorithm of which was developed using the electromagnetic theory [20]. A relief depth is determined based on optimization of diffraction grating efficiency for the specified spectral range.

Some combinations of sensors manufactured by various technologies, each for its own spectral range, may be used as radiation receivers. The radiation receiver may be also of a monolithic-type and would consist of several parts, where every part is manufactured by different technologies, for example, one part of the receiver may be made of silicon-based elements, and the other part is made of InGaAs/InP elements. Physical parameters of the selected radiation receivers are  $6.6 \times 8.8$  mm. The slit length of each channel corresponds to the detector spatial size.

A general calculation procedure for calculating design data shall be conducted as follows. First, we shall establish the angle  $\bar{\alpha}_3$  sufficient to avoid vignetting and maintaining a safety allowance; it was selected as being equal to  $15^\circ$ . Then, using the above formulas to be applied in the following order: (21), (14), (24), (1), (22), (11), (10), (15), (7), (8), the system was calculated for the first slit with the range of 400–1100 nm having assumed the central wavelength being equal to 750 nm. After that, having calculated parameters for the center wavelength from the second range of 1000–1700 nm, and having resolved an inverse problem for the mirror radii calculated for the first slit, we shall obtain values for the location and the slope of the object plane of the second slit. As demonstrated below, this slope angle will be common for both slits. The calculations were made using MS Excel software (it was selected due to its calculating simplicity using the iteration method), and then we used the obtained design values for simulation in the software package to analyze and design optical systems – ZEMAX [21].

Table 1. Basic design data

Surface type	Radius R, mm	Thickness d, mm	Glass
Object plane	$\infty$	140,6	–
1. Standard	-147,21	-71,78	Mirror
Coordinate brake	–	–	– / $1,67^\circ$
STO Diffraction grating	-75,43	65,75	Mirror
3. Standard	-141,18	-146,27	Mirror
Image plane	$\infty$	–	–

The calculation results are given in Table 1; here, the distance CO for the first slit is equal to 43.61 mm, for the second slit – to 49.27 mm. The simulation results are given in Fig. 5–6. Fig. 5 allows us to evaluate point aberration images in the image plane for the wavelength of  $1 \mu\text{m}$  in field points for the first slit:  $-8.8$  mm;  $-4.4$  mm;  $0$  mm; and for the second slit:  $1$  mm;  $5.4$  mm;  $9.8$  mm, with regard to two-dimensionality of the slits (the slit width was selected as being equal to  $12 \mu\text{m}$ ).

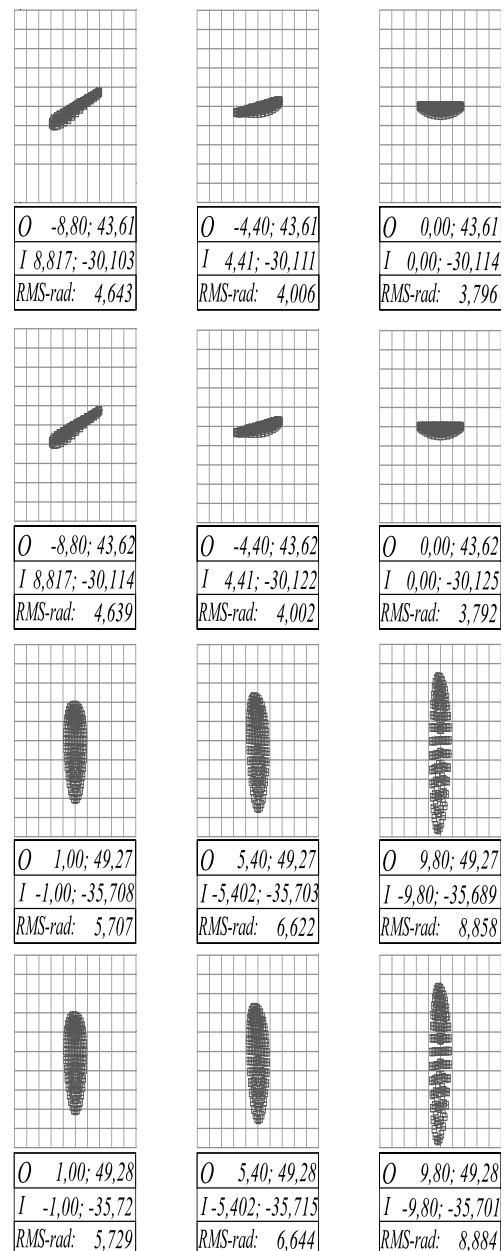
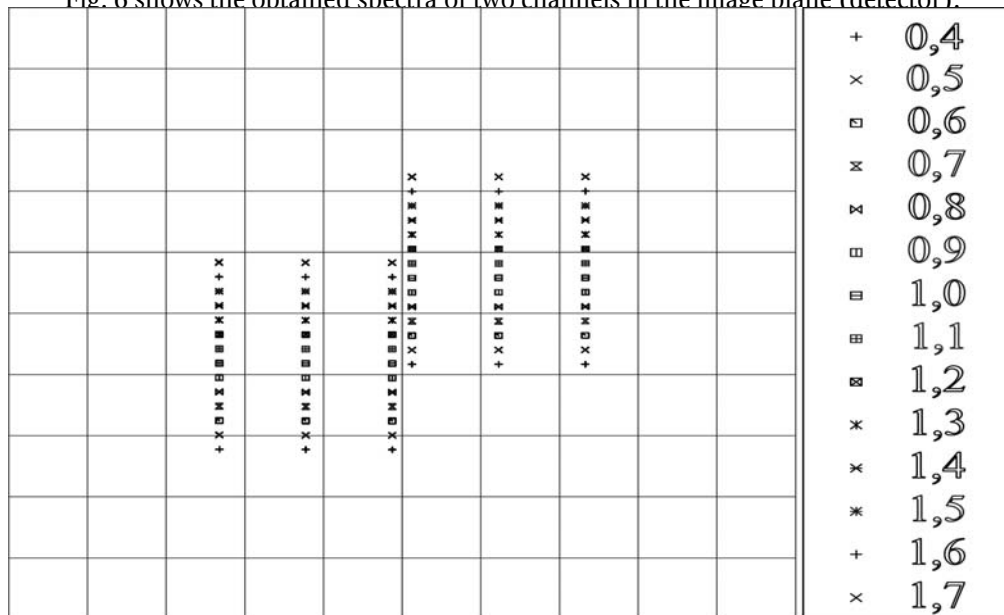


Fig. 5. Point aberration images in the image plane for the wavelength of  $1 \mu\text{m}$ .  $O$  is the object (slit),  $I$  is the image (on a matrix), the coordinates are given in mm. RMS-rad is the root mean square radius spot, in  $\mu\text{m}$

Fig. 6 shows the obtained spectra of two channels in the image plane (detector).

Fig.6. The spectra obtained in the image plane. The wavelengths are given in  $\mu\text{m}$  (on the right)

As can be seen, both spectra, the 1<sup>st</sup> and the 2<sup>nd</sup> ones, being obtained with two entrance slits, shall have various ranges of wavelengths, respectively, notwithstanding the fact that both spectra shall disperse from the diffraction grating at similar angles. The general wavelength range for the spectra of these two channels is more than the wavelength range in the spectrum of any, no matter which, channel. If a light source comes on both entrance channels, the light may be analyzed within a wider spectral range than when using a conventional, i.e. one-channel, dispersion spectrometer.

Based on the simulation modeling results, it was shown that this scheme may be applied when designing the most advanced multichannel hyperspectrometers. Its advantages, i.e. compact sizes and small weight, high light-gathering power and considerable correction of aberrations, as well as work with comparatively wide spectral range and high spatial resolution, enable to obtain high-quality hyperspectral images to solve a wide range of problems.

## References

1. Agapov, VM. In orbit, the new spacecraft observations. News of Cosmonautics, 2000; 5: 22-23.
2. Gorbunov, GG, Demin, AV, Nikiforov, VO, Sawicki, AM, Skvortsov, YS, Sokolsky, MN, Tregub, VP. Hyperspectral equipment for remote sensing. Opt., 2009; 76: 75-82.
3. Schwengerdt, RA. Remote Sensing. Models and Methods for Image Processing. Burlington MA: Elsevier Inc. Publishers, 2007.
4. Kazanskiy, NL, Kharitonov, SI, Doskolovich, LL, Pavelyev, AV. Modeling the performance of a spaceborne hyperspectrometer based on the Offner scheme. Computer Optics, 2015; 39 (1): 70-76.
5. Offner, A. New Concepts in Projection Mask Aligners. The Perkin, Elmer Corporation. Optical Engineering, 1975; 14 (2):130-132.
6. Offner, A. Annular field systems and the future of optical microlithography. The Perkin, Elmer Corporation Microlithography Division. Optical Engineering, 1987; 26 (4): 294-299.
7. Chrisp, M.P. Convex diffraction grating imaging spectrometer. Patent No. US 5880834 A. Date of Publication 9.03.1999.
8. Karpeev, SV, Khonina, SN, Kharitonov, SI. Fabrication and study of the diffraction grating on a convex surface for spectral instrument. Computer Optics, 2015; 39 (2): 211-217.
9. Mouroulis, P, Wilson, DW, Maker, PD, Muller RE. Convex grating types for concentric imaging spectrometers. Applied Optics, 1998; 37 (31): 7200-7208.
10. Richard, E, Wilson, D, Maker, P, Muller, R. Jet. Electron-Beam Fabrication of Analog-Relief Diffractive Optics on Non-Flat Substrates at Jet Propulsion Laboratory. Conference Paper Propulsion Lab., California Inst. of Tech, 2002.
11. Bruk, A, Zhikharev, EN, Streltsov, DR, Kalnov, VA, Spirin, AV, Rogozhin, AE. Some peculiarities of a new method of microrelief creation by the direct electron-beam etching of resist. Computer Optics, 2015; 39 (2): 204-210.
12. Optics of spectral devices. IV Peysahson. Ed. 2nd, ext. and rev. L.: Engineering, 1975: 312 p.
13. Malyshev, VI. Introduction to experimental spectroscopy.

M.: Nauka. Main editorial office of Physical and mathematical literature, 1979: 480 p.

■ **14.** Tarasov, KI. Designing of spectroscopic equipment. M.: Engineering, 1980: 216 p.

■ **15.** Prieto-Blanco, X, Gonzalez-Nuez, H, de la Fuente R. Off-plane anastigmatic imaging in Offner spectrometers. *Journal of the Optical Society of America A*, 2011; 28: 2332-2339.

■ **16.** Golovin, AD, Demin, AV. Compact hyperspectrometer for visible and SWIR wavelength range. *Izvestiya Vysshikh Uchebnykh Zavedeniy. Priborostroenie*, 2015; 58 (11): 869-873. (in Russian). DOI: 10.17586/0021-3454-2015-58-11-869-873.

■ **17.** Bo Yang, Chenglin Liu, Xuezhuan Ding, Xin Wang, Yin-nian Liu. Blaze Wavelength of Convex Blazed Grating in an Offner Spectrometer. *SPIE Proceedings*, 2012; 7655.

■ **18.** Greisukh, GI, Ezhov, EG, Kazin, SV, Sidyakina, ZA, Stepanov, SA. Visual assessment of the influence of adverse diffraction orders on the quality of image formed by the refractive - diffractive optical system. *Computer Optics*, 2014; 38 (3): 418-424.

■ **19.** Yu Cheng, Quan Liu, Jianhong Wu. Groove profile modification of convex blazed gratings by dip (spin) coating with photoresist. *SPIE Proceedings*, 2014; 9047.

■ **20.** PCGrate-S(X) - software for calculations of diffraction efficiency of different types of relief gratings on PCs. [Electronic resource]. URL: <http://www.pcgrate.com/>

■ **21.** ZEMAX Optical Design Program - software package for analysis and designing of optical systems. [Electronic resource]. URL: <https://www.zemax.com/>

